Electronic Supplementary Material (ESI) for Physical Chemistry Chemical Physics.

SUPPORTING INFORMATION

SABRE Enhancement with Oscillating Pulse Sequences: Symmetry Reduces Robustness

Xiaoqing Li, Jacob R. Lindale, Shannon L. Eriksson, Warren S. Warren*

Abstract: SABRE (Signal Amplification by Reversible Exchange) methods provide a simple, fast, and cost-effective method to hyperpolarize a wide variety of molecules in solution, and have been demonstrated with protons and, more recently, with heteronuclei (X-SABRE). The conventional analysis of the SABRE effect is based on level anti-crossings (LACs), which requires very low magnetic fields (~ 0.6μT) to achieve resonance and transfer spin order from the para-hydrogen to target heteronuclei. We have demonstrated in our recent study that the validity of LACs used in SABRE is very limited, so the maximum SABRE polarization predicted with LACs is not correct. Here, we present several oscillating pulse sequences that use magnetic fields far away from the resonance condition and can commonly triple the polarization. An analysis with average Hamiltonian theory indicates that the oscillating pulse, in effect, adjusts the J-couplings between hydrides and target nuclei and that a much weaker coupling produces maximum polarization. This theoretical treatment, combined with simulations and experiment, show substantial magnetization improvements relative to traditional X-SABRE methods. It also shows that, in contrast to most pulse sequence applications, waveforms with reduced time symmetry in the toggling frame make magnetization generation more robust to experimental imperfections.

SUPPORTING INFORMATION

Table of Contents

Higher-order Average Hamiltonian of AA'B System

In the theoretical section of the article, we ignore the higher-order approximation of the average Hamiltonian[1,2] and only discuss the zero-order Magnus expansion. Here, we will correct this omission. The first and second orders of the Magnus expansion are given by

$$\bar{\mathcal{H}}^{(1)} = \frac{1}{2iT}\int_0^T dt_1 \int_0^{t_1} dt_2 \,[\tilde{\mathcal{H}}(t_1), \tilde{\mathcal{H}}(t_2)] \tag{S1}$$

$$\bar{\mathcal{H}}^{(2)} = \frac{1}{6T}\int_0^T dt_1 \int_0^{t_1} dt_2 \int_0^{t_2} dt_3 \,\{[\tilde{\mathcal{H}}(t_1), [\tilde{\mathcal{H}}(t_2), \tilde{\mathcal{H}}(t_3)] + [[\tilde{\mathcal{H}}(t_1), \tilde{\mathcal{H}}(t_2)], \tilde{\mathcal{H}}(t_3)]\} \tag{S2}$$

In the square pulse and the sine wave cases, since $\tilde{\mathcal{H}}(t)$ is symmetric, $\tilde{\mathcal{H}}(t) = \tilde{\mathcal{H}}(T-t)$ for any $0 \le t \le T$, all odd order Magnus expansions are zero. Here, we give the commutation relation of $[\tilde{\mathcal{H}}(t_1), \tilde{\mathcal{H}}(t_2)]$ and $\left[[\tilde{\mathcal{H}}(t_1), \tilde{\mathcal{H}}(t_2)], \tilde{\mathcal{H}}(t_3)\right]$, based on which $\bar{\mathcal{H}}^{(1)}$ and $\bar{\mathcal{H}}^{(2)}$ can be calculated with integral computations.

$$\begin{aligned}[\tilde{\mathcal{H}}(t_1), \tilde{\mathcal{H}}(t_2)] = {} & \frac{i}{2}\Delta\omega_0 J_{HL}\{(M(t_1)-M(t_2))(\hat{I}_{1x}\hat{L}_y - \hat{I}_{1y}\hat{L}_x) \\ & + (N(t_1)-N(t_2))(\hat{I}_{1x}\hat{L}_x + \hat{I}_{1y}\hat{L}_y)\} \\ & + \frac{i}{2}J_{HH}J_{HL}(M(t_1)-M(t_2))\{\hat{I}_{1z}(\hat{I}_{2x}\hat{L}_y - \hat{I}_{2y}\hat{L}_x) + \hat{I}_{2z}(\hat{I}_{1y}\hat{L}_x - \hat{I}_{1x}\hat{L}_y)\} \\ & + \frac{i}{2}J_{HH}J_{HL}(N(t_1)-N(t_2))\{\hat{I}_{1z}(\hat{I}_{2x}\hat{L}_x + \hat{I}_{2y}\hat{L}_y) - \hat{I}_{2z}(\hat{I}_{1x}\hat{L}_x + \hat{I}_{1y}\hat{L}_y)\} \\ & + iJ_{HL}^2(M(t_1)N(t_2) - N(t_1)M(t_2))(\hat{I}_{1z} - \hat{L}_z)\end{aligned} \tag{S3}$$

$$\begin{aligned}\left[[\tilde{\mathcal{H}}(t_1), \tilde{\mathcal{H}}(t_2)], \tilde{\mathcal{H}}(t_3)\right] = {} & J_{HL}\left\{\left(\frac{(\Delta\omega_0)^2}{4} + \frac{J_{HH}^2}{2}\right)(M(t_1)-M(t_2)) + J_{HL}^2(M(t_1)N(t_2) - N(t_1)M(t_2))N(t_3)\right\}(\hat{I}_{1x}\hat{L}_x \\ & + \hat{I}_{1y}\hat{L}_y) \\ & + J_{HL}\left\{\left(\frac{(\Delta\omega_0)^2}{4} + \frac{J_{HH}^2}{2}\right)(N(t_2)-N(t_1)) + J_{HL}^2(M(t_1)N(t_2) - N(t_1)M(t_2))M(t_3)\right\}(\hat{I}_{1x}\hat{L}_y - \hat{I}_{1y}\hat{L}_x) \\ & + \frac{\Delta\omega_0}{2}J_{HH}J_{HL}(M(t_1)-M(t_2))\left(\hat{I}_{1z}(\hat{I}_{2x}\hat{L}_x + \hat{I}_{2y}\hat{L}_y) - \hat{I}_{2z}(\hat{I}_{1x}\hat{L}_x + \hat{I}_{1y}\hat{L}_y)\right) \\ & + \frac{\Delta\omega_0}{2}J_{HH}J_{HL}(N(t_1)-N(t_2))\left(\hat{I}_{1z}(\hat{I}_{2x}\hat{L}_y - \hat{I}_{2y}\hat{L}_x) + \hat{I}_{2z}(\hat{I}_{1y}\hat{L}_x - \hat{I}_{1x}\hat{L}_y)\right) \\ & + \left(\frac{J_{HH}}{2} - \frac{J_{HL}}{4}\right)J_{HH}J_{HL}\{(M(t_2)-M(t_1))(\hat{I}_{2x}\hat{L}_x + \hat{I}_{2y}\hat{L}_y) + (N(t_2)-N(t_1))(\hat{I}_{2y}\hat{L}_x - \hat{I}_{2x}\hat{L}_y)\} \\ & + \frac{J_{HH}(J_{HL})^2}{4}\{(M(t_2)-M(t_1))M(t_3) - (N(t_2)-N(t_1))N(t_3)\}(\hat{I}_{1x}\hat{I}_{2x} + \hat{I}_{1y}\hat{I}_{2y} + 2\hat{I}_{1z}\hat{I}_{2z} - 2\hat{I}_{2z}\hat{L}_z) \\ & + \frac{J_{HH}(J_{HL})^2}{4}\{(N(t_2)-N(t_1))M(t_3) - (M(t_2)-M(t_1))N(t_3) + 2(M(t_1)N(t_2) - N(t_1)M(t_2))\}(\hat{I}_{1x}\hat{I}_{2y} - \hat{I}_{1y}\hat{I}_{2x})\end{aligned} \tag{S4}$$

However, to visualize the effect of the higher order average Hamiltonian, we plot how each matrix element varies with the pulse period T in Figure S1. The pulse period T should not be too long in most SABRE[3-6] systems with reasonable exchange rate (usually $\le 50\text{s}^{-1}$), otherwise the SABRE complex only experiences a constant high magnetic field during its lifetime. Therefore, we are only interested in pulse periods that are smaller or comparable to the lifetime of SABRE complex. For the sake of conciseness, here we only study one highly symmetric pulse, square pulse, and one less symmetric pulse--ramp. In addition, we only display the result of one subspace which is displayed in Figure S1; the other one has similar behavior. Since we only calculated the first and second order approximation, all the curves refer to the subspace of $\bar{\mathcal{H}}^{(1)} + \bar{\mathcal{H}}^{(2)}$. In the zero-order case, only the non-secular matric elements which connect the α_L states and β_L states are altered, and the resulting Ms and Ns are identical. However, for the higher orders, diagonal elements are tuned as well, which is caused by the term $\hat{I}_{1z} - \hat{L}_z$ in the first order average Hamiltonian and the term $2\hat{I}_{1z}\hat{I}_{2z} - 2\hat{I}_{2z}\hat{L}_z$ in the second order (see equation (3) and (4)). Moreover, the Ms and Ns diverge in the higher order approximation. However, it is obvious that higher order average Hamiltonian are too small to rise obvious function (Figure S1). In conclusion, the zero order Magnus expansion is indeed a reliable approximation of the whole average Hamiltonian.

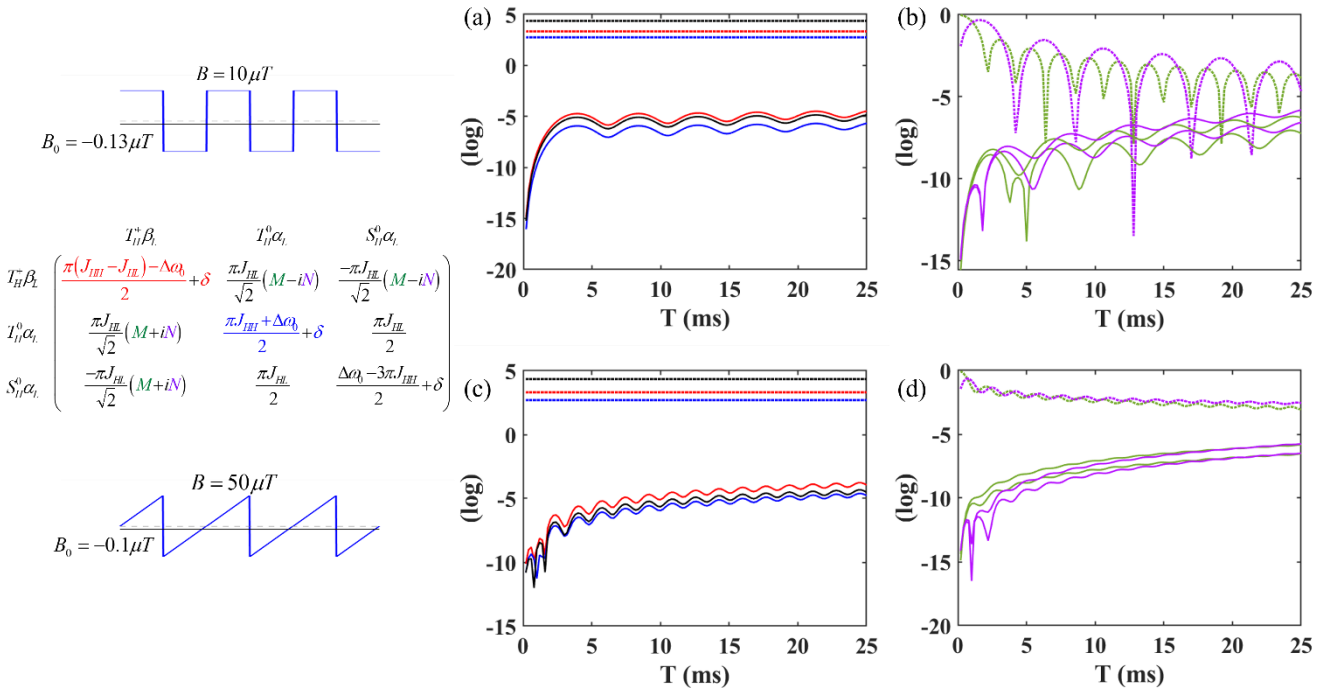

Figure S1. Plot of matrix elements in the effective Hamiltonian for a square pulse sequence (top) and ramp pulse sequence (bottom). The left and the right subplot column indicate how the three diagonal elements (left) and the adjustable coefficents M and N (right) change with the pulse period T. In all cases the dotted lines represent the zero order results while the full curves correspond to all higher orders (full numerical solution minus zero order). Because the higher order terms are almost always at least two orders of magnitude smaller than their zero-order counterparts, they are neglected in our theoretical analysis.

M and N of a symmetric triangle pulse

In the article, we conclude that for an oscillating pulse which is symmetric both about the center of each repeating interval and the center of each half cycle, its corresponding M_0 and N_0 inevitably vanish together. Here, we provide a further verification by calculating one more example, a symmetric triangle pulse. Figure S2 shows how the curves of M_0, N_0 and $\sqrt{M_0^2 + N_0^2}$ of a symmetric triangle pulse vary as a function of θ (the rotation angle in half a period), respectively. The offset field is fixed at $-0.13\mu T$. When $\theta = (2n + 1)\pi$, $M_0 = 0$, and when $\theta = 2n\pi$, $N_0 = 0$. Somewhere between $(2n - 1)\pi$ and $2n\pi$, M_0 and N_0 vanish together. All of the above features agree with the analysis and proof given in the theory section of the article. Not that this triangle pulse gives M_0 and N_0 behaviors which are quite different from those of the Ramp pulse and nearly the same as those of the sine wave and square pulse, which indicates that the symmetry plays the key role.

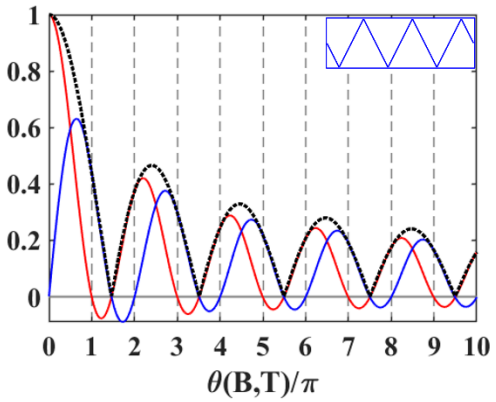

Figure S2. A depiction of how M_0 (red curve), N_0 (blue curve) and $\sqrt{M_0^2 + N_0^2}$ (black dotted curve) of the symmetric triangle pulse vary as a function of the rotation angle in half a period, respectively. We maintain the offset field at $-0.13\mu T$.

Validity of Level Anti-crossings

Level anti-crossings[7,8] are a useful tool in many spectroscopic applications. For the last decade, they have been widely used in SABRE system to predict or explain the optimal magnetic field used in SABRE experiments. In the article we show that LAC works properly for our oscillating pulse SABRE-SHEATH[5, 6] even though it does not for CW SABRE-SHEATH[11]. Here, to support our conclusion we introduce a new model – a AA'B system with the coupling between the two hydrides being positive, $J_{HH} = 8\text{Hz}$, while $J_{HL} = -25\text{Hz}$ stays unchanged. A square pulse with amplitude $B = 10\mu\text{T}$ is applied the spin system. Figure S3(a) depicts how polarization varies with both the offset field and the pulse period, in which the optimal offset field is about $\pm 0.38\mu\text{T}$. Figure S3(b) displays the LACs of one 3×3 subspace with pulse period being fixed at the optimal value, 3.6ms, and the offset field changing from 0 to $0.4\mu\text{T}$. The circled LAC at $B_0 \sim 0.37\mu T$ agrees greatly with the optimal offset field. Therefore, the validity of LACs in Oscillating Pulse SABRE-SHEATH is verified again.

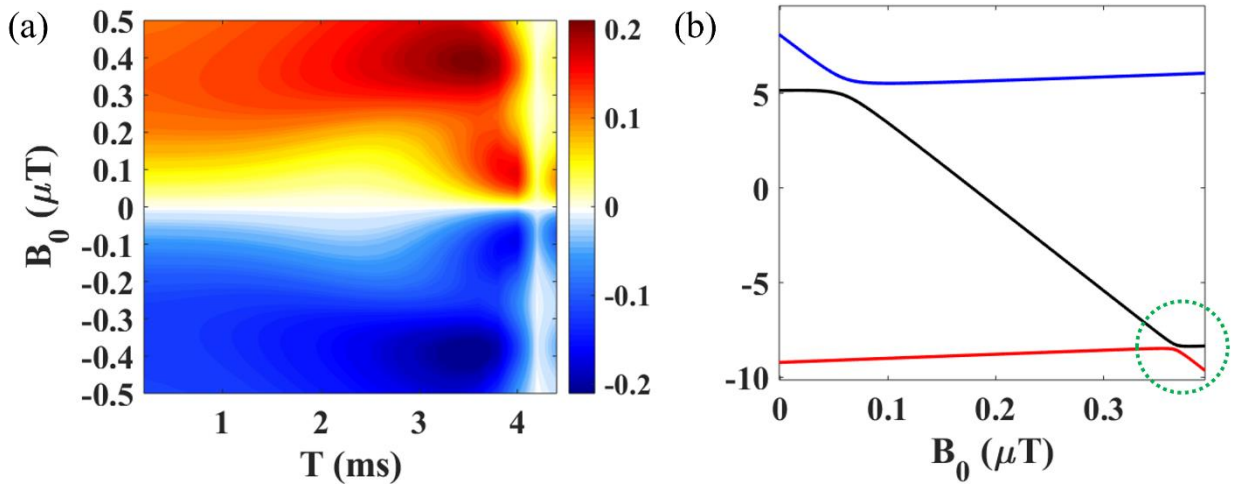

Figure S3. Experimental optimum agrees with the prediciton of LAC. The square pulse we use has a stable amplitude $10\mu T$ while changing offset and pulse period. (a) displays polarizaiton as a funtion of both offset and pulse period. The optimal offset and the optimal pulse period are $B_0 = \pm 0.38\mu T, T = 3.6ms$. (b) is the corresponding LACs of one of the 3×3 subspaces. The circle LAC occurs near $B_0 \sim 0.37\mu T$.

Zero-order Average Hamiltonian of AA'BB' system

In the paper we demonstrated that the oscillating pulse makes the coupling between hydrides and target nuclei are adjustable in the case of 3-spin system AA'B. Here we extend this conclusion to symmetric AA'BB' system. The original full Hamiltonian of the 4-spin system experiencing an unbalanced squared pulse is

$$\widetilde{\mathcal{H}}_{prime}(t) = -\big(B_0 + B(t)\big)\big(\gamma_H(\hat{I}_{1z} + \hat{I}_{2z}) + \gamma_L(\hat{L}_{1z} + \hat{L}_{2z})\big) + 2\pi J_{HH}(\vec{I}_1 \cdot \vec{I}_2) + 2\pi J_{HL}(\vec{I}_1 \cdot \vec{L}_1) + 2\pi J_{HL}(\vec{I}_2 \cdot \vec{L}_2) \quad \text{(S5)}$$

In the same way as the 3-spin case, we rearrange the formula in the following

$$\widetilde{\mathcal{H}}_{rearranged}(t) = -\big(B_0 + B(t)\big)\gamma_H(\hat{I}_{1z} + \hat{I}_{2z} + \hat{L}_{1z} + \hat{L}_{2z}) + \big(\Delta\omega_0 + \Delta\omega(t)\big)(\hat{L}_{1z} + \hat{L}_{2z}) + 2\pi\{J_{HH}(\vec{I}_1 \cdot \vec{I}_2) + J_{HL}(\vec{I}_1 \cdot \vec{L}_1) + J_{HL}(\vec{I}_2 \cdot \vec{L}_2)\} \quad \text{(S6)}$$

in which $\Delta\omega_0 = B_0(\gamma_H - \gamma_L)$, and $\Delta\omega(t) = B(t)(\gamma_H - \gamma_L)$. Similarly, simplify the Hamiltonian by taking out the first term which commutes with the rest of the Hamiltonian.

$$\widetilde{\mathcal{H}}(t) = \big(\Delta\omega_0 + \Delta\omega(t)\big)(\hat{L}_{1z} + \hat{L}_{2z}) + 2\pi\{J_{HH}(\vec{I}_1 \cdot \vec{I}_2) + J_{HL}(\vec{I}_1 \cdot \vec{L}_1) + J_{HL}(\vec{I}_2 \cdot \vec{L}_2)\} \quad \text{(S7)}$$

Transfer this Hamiltonian to the toggling frame $U(t) = \exp\left(-i(\hat{L}_{1z} + \hat{L}_{2z})\int_0^t \Delta\omega(t')\,dt'\right)$

$$\begin{aligned}\widetilde{\mathcal{H}} &= U\{\Delta\omega_0(\hat{L}_{1z} + \hat{L}_{2z}) + 2\pi J_{HH}(\vec{I}_1 \cdot \vec{I}_2) + 2\pi J_{HL}(\vec{I}_1 \cdot \vec{L}_1) + 2\pi J_{HL}(\vec{I}_2 \cdot \vec{L}_2)\}U^\dagger \quad \text{(S8)}\\ &= \Delta\omega_0(\hat{L}_{1z} + \hat{L}_{2z}) + 2\pi J_{HH}(\vec{I}_1 \cdot \vec{I}_2) + 2\pi J_{HL}\left(\hat{I}_{1z}\hat{L}_{1z} + M(t)\big(\hat{I}_{1x}\hat{L}_{1x} + \hat{I}_{1y}\hat{L}_{1y}\big) + N(t)\big(\hat{I}_{1x}\hat{L}_{1y} - \hat{I}_{1y}\hat{L}_{1x}\big)\right)\\ &+ 2\pi J_{HL}\left(\hat{I}_{2z}\hat{L}_{2z} + M(t)\big(\hat{I}_{2x}\hat{L}_{2x} + \hat{I}_{2y}\hat{L}_{2y}\big) + N(t)\big(\hat{I}_{2x}\hat{L}_{2y} - \hat{I}_{2y}\hat{L}_{2x}\big)\right)\end{aligned}$$

Since there are two target nuclei in every SABRE complex, and each one couples with one of the two hydrides, these two couplings are adjusted identically by the oscillation pulse. The time dependent coefficients are $M(t) = \cos\left(\int_0^t \Delta\omega(t')\,dt'\right)$, and $N(t) = \sin\left(\int_0^t \Delta\omega(t')\,dt'\right)$, which are the same with the 3-spin case. Therefore, the zero-order average Hamiltonian is easy to work out.

$$\widehat{\mathcal{H}}^{(0)} = \Delta\omega_0(\hat{L}_{1z} + \hat{L}_{2z}) + 2\pi J_{HH}(\vec{I}_1 \cdot \vec{I}_2) + 2\pi J_{HL}\left(\hat{I}_{1z}\hat{L}_{1z} + M_0(\hat{I}_{1x}\hat{L}_{1x} + \hat{I}_{1y}\hat{L}_{1y}) + N_0(\hat{I}_{1x}\hat{L}_{1y} - \hat{I}_{1y}\hat{L}_{1x})\right) \quad \text{(S9)}$$
$$+ 2\pi J_{HL}\left(\hat{I}_{2z}\hat{L}_{2z} + M_0(\hat{I}_{2x}\hat{L}_{2x} + \hat{I}_{2y}\hat{L}_{2y}) + N_0(\hat{I}_{2x}\hat{L}_{2y} - \hat{I}_{2y}\hat{L}_{2x})\right)$$

where $M_0 = \frac{\sin(\Delta\omega T/2)}{\Delta\omega T/2}$ and $N_0 = \frac{1-\cos(\Delta\omega T/2)}{\Delta\omega T/2}$. If $\Delta\omega T/2 = 2n\pi$, the coupling between hydride and the target nulcei vanish. Therefore, the resulting polarization is zero, as what is shown in Figure S4, along the vertical line of $T = 4.3ms$ the offset field B_0 and the pulse period T are scanned to figure out the optimal condition which is $B_0 = -0.16\mu T$, and $T = 4ms$, while the pulse amplitude B is pinned at $10\mu T$. Compared with the 3-spin system, the optimal offset shifted a little bit which is caused by the different spin construction of the SABRE complex, but the optimal pulse period stays the same since J_{HL} is tuned identically in both 3-spin and 4-spin cases. The subspaces of the average Hamiltonian associated with spin transfer are displayed in equation (S13). The basis used here is a singlet-triplet basis for both the AA' pair and the BB' pair. The couplings between the states of the target spins with respect to zero spin angular momentum projection (S_L^0, T_L^0) and states with a nonzero projection are adjustable. This fact is significant becasue the population transfer between these states, which is directly affected by the coupling strength, generates polarization, while the coupling between states S_L^0 and T_L^0 stays unchanged, and the coupling between states T_L^+ and T_L^- is always zero.

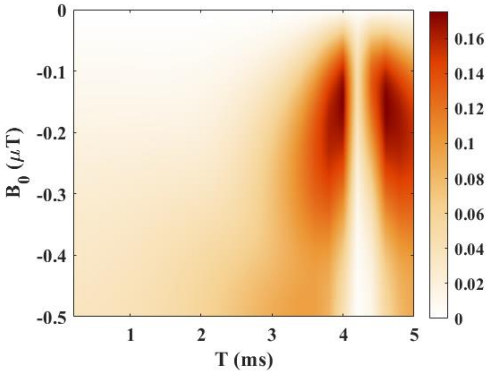

Figure S4. Polarization of a AA'BB' system under an unbalanced square pulse varies as the pulse period and the offset field. We hold the pulse amplitude, $B = 10\mu T$, and the accordingly optimal condition is $B_0 = -0.16\mu T$, and $T = 4ms$. Simulation parameters: coupling strength $J_{HH} = -8Hz$, $J_{HL} = -25Hz$, exchange rates $k_L = 24s^{-1}$, $k_H = 8s^{-1}$, [catalyst]:[ligand]=1:10.

$$\begin{array}{c} \\ T_H^+S_L^0 \\ S_H^0T_+^0 \end{array} \begin{array}{c} \begin{array}{cc} T_H^+S_L^0 & S_H^0T_+^0 \end{array} \\ \begin{pmatrix} \frac{\pi J_{HH}}{2} & \pi J_{HL}(M_0 - iN_0) \\ \pi J_{HL}(M_0 + iN_0) & -\frac{3\pi J_{HH}}{2} - \Delta\omega_0 \end{pmatrix} \end{array}$$

$$\begin{array}{c} \\ T_H^-S_L^0 \\ S_H^0T_L^- \end{array} \begin{array}{c} \begin{array}{cc} T_H^-S_L^0 & S_H^0T_L^- \end{array} \\ \begin{pmatrix} \frac{\pi J_{HH}}{2} & \pi J_{HL}(M_0 + iN_0) \\ \pi J_{HL}(M_0 - iN_0) & -\frac{3\pi J_{HH}}{2} + \Delta\omega_0 \end{pmatrix} \end{array}$$

$$\begin{array}{c} \\ T_H^+T_L^- \\ T_H^0T_L^0 \\ S_H^0S_L^0 \\ T_H^-T_L^+ \end{array} \begin{array}{c} \begin{array}{cccc} T_H^+T_L^- & T_H^0T_L^0 & S_H^0S_L^0 & T_H^-T_L^+ \end{array} \\ \begin{pmatrix} \frac{\pi(J_{HH} - 2J_{HL})}{2} + \Delta\omega_0 & \pi J_{HL}(M_0 - iN_0) & -\pi J_{HL}(M_0 - iN_0) & 0 \\ \pi J_{HL}(M_0 + iN_0) & \frac{\pi J_{HH}}{2} & \pi J_{HL} & \pi J_{HL}(M_0 - iN_0) \\ -\pi J_{HL}(M_0 + iN_0) & \pi J_{HL} & -\frac{3\pi J_{HH}}{2} & -\pi J_{HL}(M_0 - iN_0) \\ 0 & \pi J_{HL}(M_0 + iN_0) & -\pi J_{HL}(M_0 + iN_0) & \frac{\pi(J_{HH} - 2J_{HL})}{2} - \Delta\omega_0 \end{pmatrix} \end{array} \quad \text{(S10)}$$

Robustness to variations of exchange rate

In the article we have already confirmed that the 3-spin system with negative J_{HH} is robust to variations of exchange rate. In this section we demonstrate with DMEx[12] simulation method that the positive J_{HH} case and 4-spin systems also have strong robustness to variations in exchange rate. Likewise, we use a square pulse sequence with $B = 10\mu T$ as an example. The optimal magnetic field of the AA'B system with $J_{HH} = 8Hz$ is $\pm 0.4\mu T$, while for the AA'BB' system with $J_{HH} = -8Hz$ the optimal filed is $\pm 0.11\mu T$. In Figure S5, we study 4 different cases with k_L changing from $1s^{-1}$ to $100s^{-1}$, but the optimal field does not obviously shift. The optimal conditions do not shift a lot in the low exchange cases. As the exchange rate of the substrate goes up, the optimal condition shifts in the direction that the offset increases while the pulse period decreases. However, the overall shift is mild. All the feature are consistent with the 3-spin case shown in the article (Figure 8).

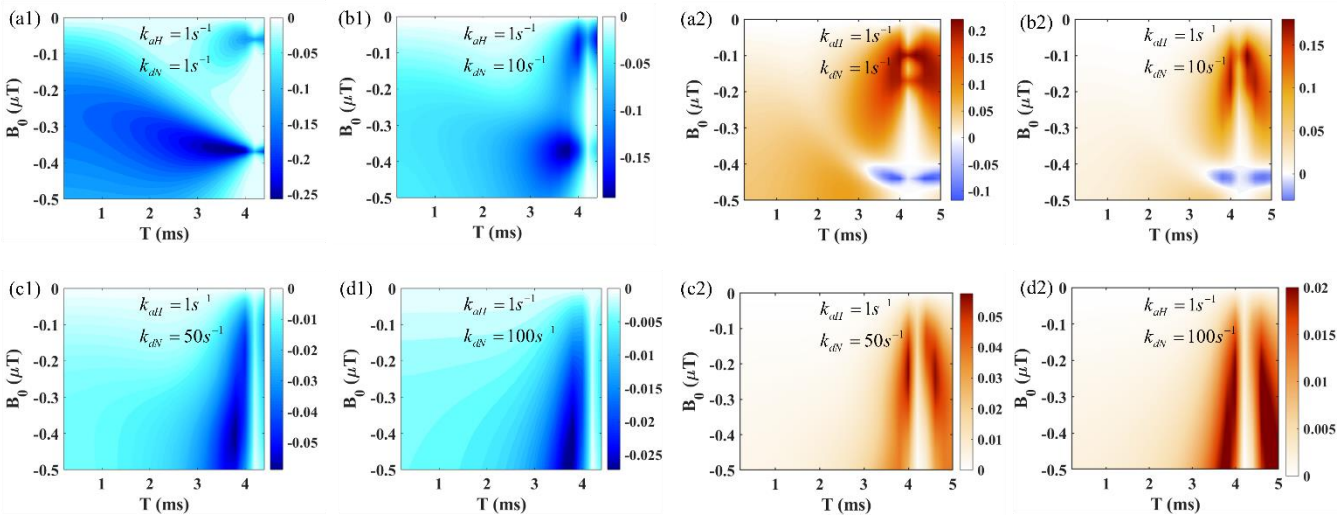

Figure S5. Optimal polarization conditions with different substrate exchange rates. The left four subplots refer to an AA'B spin system with a positive hydride coupling, $J_{HH} = 8Hz$, while the right four refer to an AA'BB' spin system with a negative hydride coupling, $J_{HH} = -8Hz$. (a1) The optimal field is -0.37μT, and the optimal period is 3.8ms. (b1) The optimal field is -0.37μT, and the optimal period is 3.8ms. (c1) The optimal field is -0.4μT, and the optimal period is 3.8ms. (d1) The optimal field is -0.44μT, and the optimal period is 3.8ms. (a2) The optimal field is -0.11μT, and the optimal period is 4.0ms. (b2) The optimal field is -0.17μT, and the optimal period is 4.0ms. (c2) The optimal field is -0.21μT, and the optimal period is 4.0ms. (d2) The optimal field is -0.5μT, and the optimal period is 3.8ms. The subplots have inconsistent color scales in order to show off more detail. Simulation parameters: coupling strength $J_{HL} = -25Hz$, [catalyst]:[ligand]=1:10.

References

[1] U. Haeberlen, J. S. Waugh, *Phys. Rev*. 1968, **175**, 453
[2] U. Haeberlen, *High Resolution NMR in Solids*, Academic, New York, 1976.
[3] R. W. Adams, J. A. Aguilar, K. D. Atkinson, M. J. Cowley, P. I. P. Elliott, S. B. Duckett, G. G. R. Green, I. G. Khazal, J. Lopez-Serrano, D. C. Williamson, *Science*. 2009, **323**, 1708.
[4] K. D. Atkinson, M. J. Cowley, P. I. P. Elliott, S. B. Duckett, G. G. R. Green, J. Lopez-Serrano, A. C. Whitwood, *J. Am. Chem. Soc*. 2009,**131**, 13362.
[5] T. Theis, M. L. Truong, A. M. Coffey, R. V. Shchepin, K. W. Waddell, F. Shi, B. M. Goodson, W. S. Warren, E. Y. Chekmenev, *J. Am. Chem. Soc.* 2015, **137**, 1404.
[6] J. R. Lindale, S. L. Eriksson, C. P. N. Tanner, Z. Zhou, J. F. P. Colell, G. Zhang, J. Bae, E. Y. Chekmenev, T. Theis, W. S. Warren, *Nature Communication*, 2019, **23**.
[7] A. N. Pravdivtsev, A. V. Yurkovskaya, H.-M. Vieth, K. L. Ivanov, R. Kaptein, *ChemPhysChem* 2013, **14**, 3327 – 3331.
[8] A. N. Pravdivtsev, A. V. Yurkovskaya, N. N. Lukzen, H.-M. Vieth, K. L. Ivanov, *Phys. Chem. Chem. Phys*. 2014, **16**, 24672-24675.
[9] J. R. Lindale, S. L. Eriksson, C. P. N. Tanner, W. S. Warren, *Sci. Adv*. 2020, **6**, 32.
[10] S. L. Eriksson, J. R. Lindale, X. Li, W. S. Warren, *Sci. Adv.* 2022 (in press)

Data and Materials Availability: All data are available in the main text or the supplementary materials and raw data are available in the Duke Research Data Repository at https://doi.org/10.7924/r4cj8j090